Solid Freeform Fabrication 2022: Proceedings of the 33rd Annual International Solid Freeform Fabrication Symposium – An Additive Manufacturing Conference
Reviewed Paper

KNOWLEDGE BASE DEVELOPMENT FOR IRON-PLA COMPOSITE FILAMENTS IN ADDITIVE MANUFACTURING

Ranger Buchanan*, Jeevan Kumar Dasari*, Ismail Fidan[¥],
Michael Allen[Ψ], and Indranil Bhattacharya[β]

*Department of Mechanical Engineering
[¥]Department of Manufacturing and Engineering Technology
[Ψ]Department of Mathematics
[β]Department of Electrical and Computer Engineering
1 William L Jones Drive
Tennessee Technological University
Cookeville, TN 38505

Abstract

Additive Manufacturing (AM) is one of the latest manufacturing processes where instead of cutting away from material or casting an object, as in Traditional Manufacturing (TM), one constructively adds material to create a required design. The benefits of AM allow for some designs that are impossible to be manufactured with TM methods. One of the most common AM processes is Fused Filament Fabrication (FFF), which utilizes layers of extruded materials to manufacture objects. While the most common materials in 3D printing are plastics, some other materials like metals can also be used. Such metallic printers can be utilized to manufacture materials with added electrical properties in addition to structural strength.

Today, several new filaments are developed, tested, and practiced to answer the growing fabrication needs of advanced manufacturing industry. Several new materials such as wood, carbon fiber, fiber glass, and Kevlar are added to filaments to create new composite ones. The beta-testing results of these new filaments have been analyzed to improve their properties and functionality. The goal of this research study is to develop a number of knowledge blocks to successfully produce Iron-PLA composite parts and analyze the mechanical and magnetic properties in addition to the energy consumption of the prints based upon print parameters.

Keywords: Fused Filament Fabrication, Iron-PLA Filament, Magnetability, ANOVA, MANOVA

Introduction

Additive manufacturing (AM) refers to manufacturing processes of constructively adding material rather than through casting or subtractive manufacturing as is common with other forms of traditional manufacturing (TM). Commonly used forms of AM processes include Stereolithography (SLA) or Vat Photopolymerization, Electron Beam Melting (EBM), and Fused Filament Fabrication (FFF). SLA uses light to solidify resin materials for its AM processes. EBM fuses material together through the use of an electron beam. FFF, also called FDM (Fused Deposition Modeling) or Material Extrusion, extrudes the filament material in layers onto a surface

using nozzles. Figure 1 presents the seven core AM technologies with their graphical representations. The research conducted in this project is to investigate the physical behaviors of Iron-PLA parts produced with the AM process, and this research study elected to utilize FFF for fabrication and testing. As it can be seen from Figure 1, FFF is a Material Extrusion process which is one the seven main AM technologies [1].

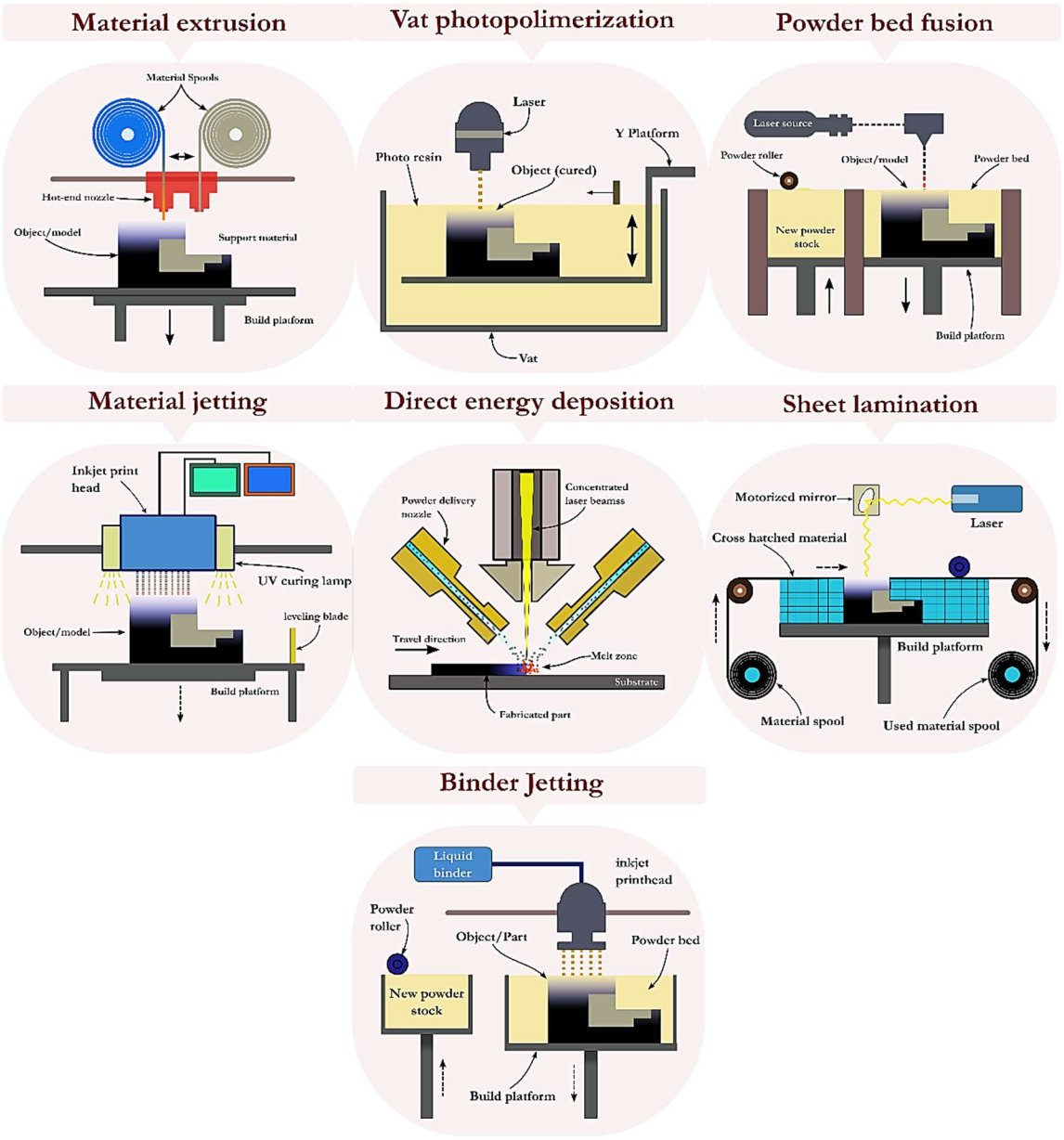

Figure 1: Main AM Technologies and Their Graphical Representation

These fields of AM have been growing significantly among industries in recent years. Wohlers Report 2022 [2] states that despite the COVID-19 pandemic, worldwide AM revenue was substantial with a 17.5% increase from 2020 to 2021. The revenue in 2020 was $5.303 billion, and $6.229 billion in 2021. Figure 2 displays revenue data (in millions of dollars) for AM products and services worldwide. Neither AM services nor products data include the use of AM for other processes like molded parts and casts. It is believed that the trend of adapting and implementing

the AM technologies into engineering fields will continue to increase sharply. The findings of this study will contribute to the AM body of knowledge in Material Extrusion, Magnetic Materials, Energy Consumption of the AM Processes, and Quality Part Production in AM.

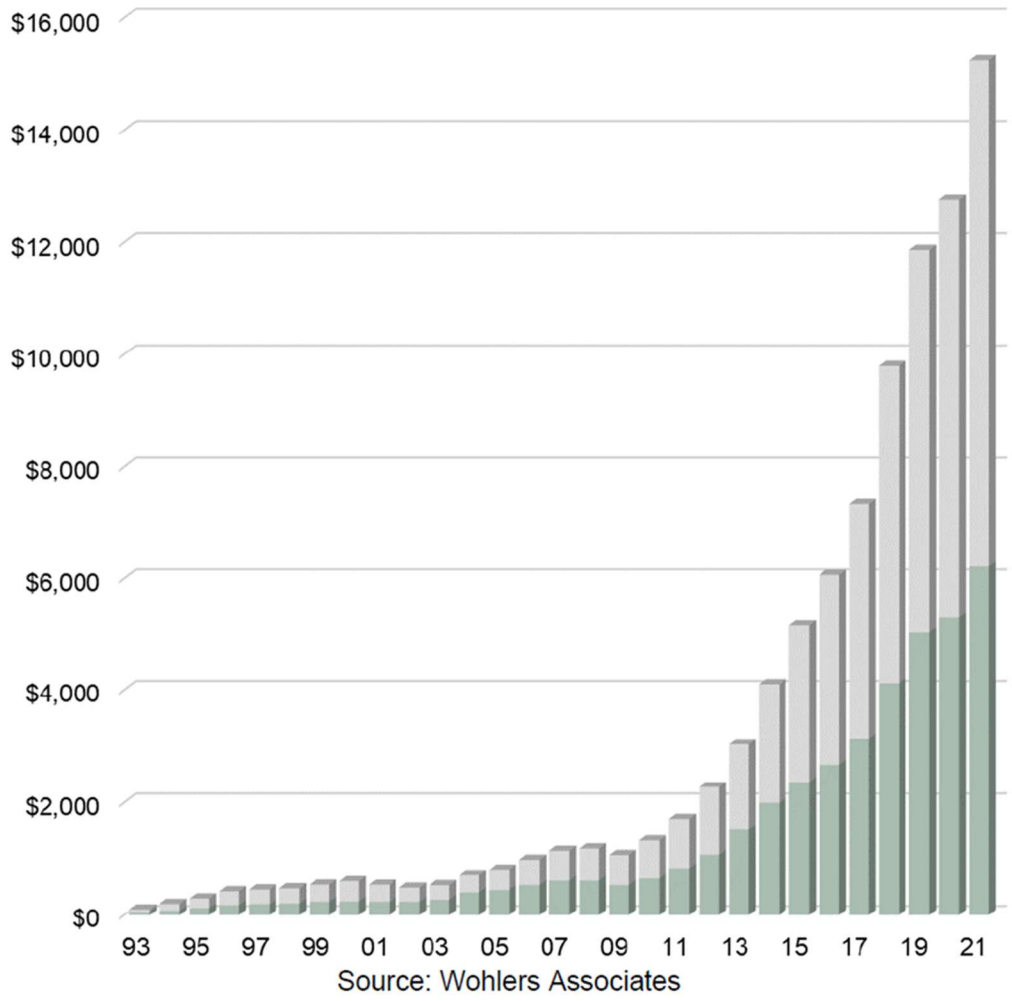

Figure 2: AM Industry Growth Data from Wohlers Report 2022. Green segments represent production while gray segments represent services.

AM utilizes many common materials; among the most commonly used AM materials are thermoplastic materials, due to their relative ease to manufacture and fairly low melting points. Some examples of thermoplastics used in AM include, Poly Lactic Acid (PLA) for the cost and ease of printing as well as Acrylonitrile Butadine Styrene (ABS) for its improved impact resistance and similar low cost. While plastic materials are the most commonly used, some AM printers can handle metal materials and composite materials. These materials can display properties that would not be present within plastics, such as conductivity or magnetability.

This research focuses on the properties of samples made by using Iron–PLA composite filaments. A number of process parameters like infill percentage, layer height, and print speed is varied to investigate the quality of products fabricated with the FFF process. By altering these process parameters, several response variables are obtained to determine potential improvements.

As of now, the magnetic properties of 3D printed objects have limited research studies. Additionally, this original study seeks to investigate different parameters that affect the fabrication cost, magnetic flux density, print time, and energy consumption of Iron-PLA parts.

In several industries, the current use of magnetic particles in AM is limited, according to Tumer's research study [3]. The study focused on additively manufactured parts in various applications of automotive, medicine, and aviation industries with the help of PLA composites. Additionally, in this investigation the authors discussed advantages of PLA composites. For the medical industry, these parts could be used as alternate parts of damaged organs according to the customer requirements.

Blakey-Milner [4] and Ulu [5] discussed the metal AM processes and their latest implementations. Blakey-Milner's research provided a comprehensive review of metal AM in the aerospace industry. Ulu's study examined producing low cost additively manufactured parts by reducing material usage with different AM techniques and explained the benefits of metal AM. Terry [6], presented similar research to the research conducted by Blakey-Milner and Ulu. Terry's work reported a number of sources presenting the ways to obtain production in lower energy consumptions and better product qualities. The study draws a general picture on AM and its potential with smart manufacturing technologies.

Chaudhary [7] and Najgebauer [8] presented the applications of magnetic particles in electrical and mechanical settings and explained how to produce soft and hard magnets with the help of AM as well as outlined the future trends of AM in day-to-day life. Najgebauer's study explained about the properties of soft and hard magnetic composites by using Nd-Fe-B material. Two different processes were applied to make the powders and as well as researching the applications in motor industries.

Henderson [9] and Watson [10] additionally explained magnetic behavior of iron PLA composites. Henderson fabricated the samples within the presence of a magnetic field and without the presence of a magnetic field. Then the study measured the samples with a vibrating sample magnetometer. The samples made within the presence of a magnetic field generated more magnetic susceptibility. Watson conducted similar research to Henderson, however, Watson's study directly deposited the magnetic particles on the sample which exhibited a larger magnetic field compared to others prints where magnetic particles were not directly deposited.

Both Guan [11] and Angelopoulos [12] discussed the tensile strength and magnetic properties of composite materials. Guan's research focused on carbonyl powder PLA composites created by FFF process and concentrated on the topics of the microstructure, tensile strength of magnetic printed particles, mechanical properties, and magnetic properties. Angelopoulos's work is similar to Guan's, and the research noted material property differences between thermoplastic and composite filaments. Angelopoulos additionally conducted work on the morphological structure of fillers in attained composite filaments.

Lu [13] and Bade [14] performed a similar kind of research study to Guan's and Angelopoulos's works, about tensile testing of PLA samples. Lu used a low-cost metal material extrusion, and produced tensile samples by using pre- and post-sintering. The research then

compared the sintered samples with pure metal specimens fabricated by other processes. The research also conducted preliminary studies of mechanical characterization of metal material extrusion. Bade's research focused on samples produced with carbon fibers with and without molded process by AM. The molded process displayed more tensile strength compared to other methods.

Maurel [15] discussed the advantages and drawbacks of thermoplastic material extrusion and polymer powder bed fusion with LiFePO4 and Polypropylene materials. The research thoroughly discussed the electrochemical, electrical, morphological, and mechanical properties of the specimens.

Murr [16] explained how EBM and SLA processes could be used in 3D imaging. The research addressed the visualization of solidification phenomena associated with EBM and SLA processes and described the fabrication of metals and alloy components that used AM.

Femi-Oyetoro [17] utilized machine learning techniques to identify the flexural properties of short fiber reinforced composites produced with FFF technology. The research determined that the results were accurate when compared to other processes.

Hasanov [18] explained the usage of rare earth metals in various industries including automotive, medical, and aerospace industries. By applying FFF process, the research produced and studied magnetic powder-infused filaments. The study provides information beneficial in low cost, efficient, and complex magnetic components' fabrication based on the application areas.

Experimental Procedure

A design of experiments structure is created in order to perform a parametric study for testing and analysis purposes of the research. The proposed structure allows for planning to help guide the experiment, which helps to avoid waste and minimize errors. Moreover, the findings of the entire study are more easily found and established with the help of the design of experiments.

This study aims to investigate low Iron-PLA filaments for magnetic properties of different process parameters of infill percentage, layer height, and print speed. With the chosen inputs, there are a total 12 possible variations, and each variation is printed with five replicates to avoid potential discrepancies. With respect to the input variables, the research study sought to investigate the print samples to find various output variables such as magnetic flux density and power consumption. The main purpose of this investigation is to test low Iron-PLA filaments for magnetic properties in order to generate knowledge blocks on the potential for magnetic materials within AM.

The experiments are conducted through the entire printing process of the samples. Data is collected from a total of 60 samples that are created with varying layer heights, print speeds, and infill densities. Print order is chosen through a randomization process to avoid selection bias and accidental bias. Samples are designed in SolidWorks [19] and saved in an STL format. After a few initial test prints, the final design is chosen to be 2 in x 1 in x 0.1 in or 50.8 mm x 25.4 mm x 2.54 mm. These dimensions are chosen to allow for quick printing of the samples and to decrease the chances of a print error. The Dremel DigiLab 3D Slicer [20] is used for slicing the solid models

generated by SolidWorks into a gcode file for the Dremel Digilab 3D Printer 3D45 [21]. AMOLEN 3D Printer Filament (20% Magnetic Iron Powder - PLA Filament 1.75mm) [22] is used for the tests. The Dremel DigiLab 3D Printer 3D45 is utilized for printing the samples for the data collection. Figure 3 represents the steps of the experimental process that are taken for this research.

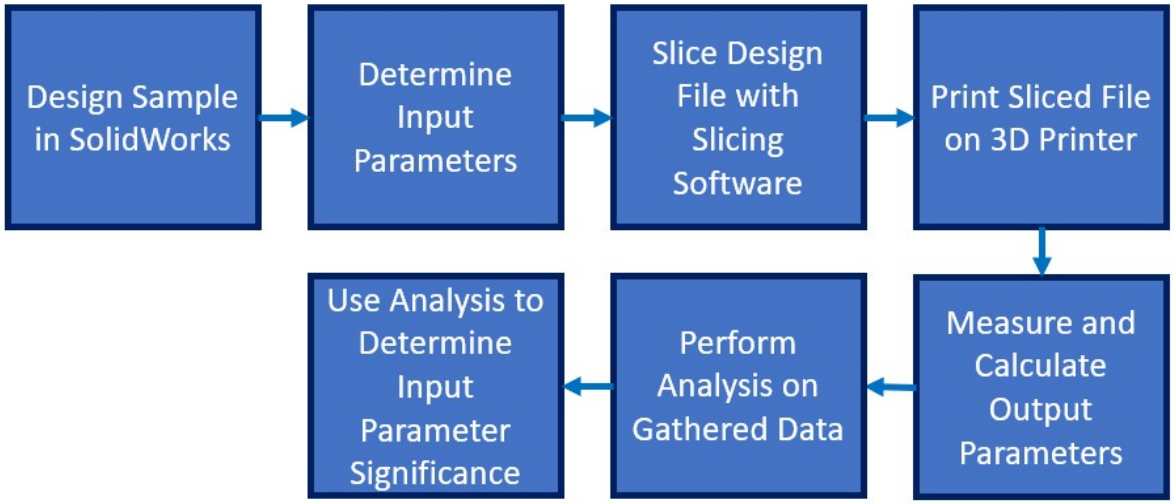

Figure 3: Experimental Process

Various equipment was used to document the output variables and their responses. The variable of printing time is documented in hours, and it covers the time of the printing process from the start of first layer to the complete fabricated part. In this study, print time is measured with the use of a stopwatch application [23] on a mobile phone. To avoid any alterations in print time caused by initial print temperature, print time is taken at the point when the material extrusion begins. The reason for this timing change is that printer takes less time to heat a hot nozzle from 200° C to 220° C than it does for the printer to heat up a nozzle from 20° C to 220° C.

A REED R5090 Power Meter [24] is used to measure the print cost of each sample. This measurement is conducted through inputting the local energy cost of 10.04 cents/kWh [25] into the device and calculating the change in cost before the start of the print and after the print is finished.

The mass of each print is measured individually using a Mettler Toledo PL602 S [26] precision balance. Before each measurement, the scale is tared to zero to avoid any erroneous measurements. Dimensional measurements of length, width, and height are collected through the use of IP54 digital calipers [27] on printed parts. Height measurements are taken along the z-axis of the print direction. Width measurements are taken along the x-axis of the print direction. Length measurements are taken along the y-axis of the print direction. These dimensional measurements are compared to the designed dimensional parameters to determine the percent difference between them and the process parameters.

Surface Roughness is the measure of change of the surface perpendicular to the surface. Surface Roughness is measured in micrometers with Mitutoyo SJ-210 Surface Roughness Equipment [28]. The Mitutoyo SJ-210 Surface Roughness Equipment measures differently

dependent on the setting, but for this test, Ra surface roughness is measured. Ra surface roughness measures the average deviation of a measured surface to produce a value. Samples are measured by keeping the part stationary as the sensor traces over the surfaces of the part. The top of the print relative to the print bed, the width, and the length of the print are all measured in these tests.

Magnetic flux density is the value of the change in the total magnetic field passing through a surface area which was measured through the use of the FW Bell Model 640 Gaussmeter [29]. The Gaussmeter measures the magnetic flux density of an object. A sample is placed perpendicularly in between the magnet and the three-axis probe, and the resulting change in the magnetic field is measured to determine the magnetic flux density of the sample. The three-axis probe is set to the z-direction, as the z-direction of the probe operates along the length of the probe. The probe holder is designed to hold the probe stationary with the magnet and the test sample at a distance of 7.5 mm between each.

Data Collection and Analysis

All data is collected into Excel for computational analysis of additional output variables. Additional analysis of the data is conducted through Statistical Analysis Software (SAS). While most prints are included within the data, some prints have been excluded due to some error, notably print 6 due to print parameter errors during manufacture, and print 51 due to extreme warping of the sample.

Input variables include the infill density, layer height, and print speed for each print. Infill density is set to have a value of either 20%, 60%, or 100% infill density. Layer height is set as 0.1 or 0.2 mm. Print speed is set as either 45 or 60 mm/s. There are five prints per batch, and each batch received a different combination of input variables. Documentation of these input variables can be found in Table 1. Local energy price is a constant 10.04 c/kWh; this value was determined by searching for the current energy price for the area. Design height was chosen to be 2.54 mm. Design width was chosen to be 50.8 mm. Design length was chosen to be 25.4 mm.

Table 1: Input Variable Parameters

Infill Density	Layer Height (mm)	Print Speed (mm/s)
20%, 60%, 100%	0.1, 0.2	45, 60

Measured output variables include any output variable measured with equipment, such as calipers or a scale. This includes print time, energy cost, magnetic flux density, dimensional variation, mass, and surface roughness. Print time was counted for each print through the use of a stopwatch app and documented in units of hours. Energy cost was measured in cents for each print with a sensor. Magnetic flux density was measured in Gauss with a 3-axis probe connected to a FW Bell Model 640 Gaussmeter. The print values for height, width, and length were all measured with Vernier calipers. Mass was measured through the use of a Mettler Toledo PL602 S precision balance. Surface Roughness of multiple surfaces was measured in micrometers with the use of Mitutoyo SJ-210 Surface Roughness equipment.

Derived output variables include any output variable that was derived using calculations with measured output variables. Percent difference and energy consumption are derived output variables. Percent difference between the dimensional measurements and their design parameters is calculated through the following equation.

$$\frac{Measured\ Dimension - Desig\ \ Dimension}{Design\ Dimension} * 100\% = Percent\ Difference \quad (1)$$

Similarly, energy consumption is a calculated variable; the REED R5090 Power Meter was set to calculate print cost per print rather than energy consumption per print. Energy consumption is then calculated through the following equation.

$$\frac{Energy\ Cost\ (¢)}{Local\ Energy\ Cost\ (¢/kWh)} = Energy\ Consumption \quad (2)$$

Analysis of the process related parameters will prove beneficial for the practitioners of the AM field could utilize these findings in their works. One major method of analysis includes using General Linear Models (GLM) with SAS. GLM uses a least squares method in order to fit a linear model. Statistical methods within a GLM process include regression, variance analysis, covariance analysis, multivariate variance analysis, and partial correlation. GLM analysis is commonly used to model relationships between input and output variables. Here, GLM are used to display a relationship between the input variables of infill density, layer height, and print speed to the output variables.

Correlation coefficients show correlations between response variables; for this data, a selected alpha value of less than 0.05 or 5% represents a significant correlation. This value was chosen for alpha as it is a fairly standard value in many other experiments. Table 2 shows a correlation table for the output variables within the test. Dimensional Difference represents an average of the absolute values of the variations within the dimensions of the samples, and Surface Roughness represents the surface roughness values of each face added together and then averaged. Based on the data shown, print time, cost, magnetic flux density, and mass are all correlated with one another, meaning that in part the output of some response variables can be gathered from the other correlated response variables.

Table 2: Correlation Coefficients Table

	Print Time	**Cost**	**Magnetic Flux Density**	**Dimensional Difference**	**Mass**	**Surface Roughness**
Print Time	1.0000	0.98640 <0.0001	0.48126 <0.0001	-0.15338 0.2504	0.35655 0.0060	-0.28296 0.0314
Cost	0.98640 <0.0001	1.0000	0.48584 <0.0001	-0.11992 0.3699	0.36586 0.0047	-0.30157 0.0214
Magnetic Flux Density	0.48126 <0.0001	0.48584 <0.0001	1.000	-0.22562 0.0886	0.88416 <0.0001	-0.10594 0.4287
Dimensional Difference	-0.15338 0.2504	-0.11992 0.3699	-0.22562 0.0886	1.0000	-0.18132 0.1731	0.06068 0.6509
Mass	0.35655 0.0060	0.36586 0.0047	0.88416 <0.0001	-0.18132 0.1731	1.0000	-0.04339 0.7464
Surface Roughness	-0.28296 0.0314	-0.30157 0.0214	-0.10594 0.4287	0.06068 0.6509	-0.04339 0.7464	1.0000

Normally, Analysis of Variance (ANOVA) could be utilized for data analysis. The correlation however, necessitates Multivariate Analysis of Variance (MANOVA) [30] because regular ANOVA does not accurately represent each response variable when the variables are correlated. The equation for this model is shown in Equation 3:

$$y_{ijkl} = \mu + \alpha_i + \beta_j + \delta_k + \alpha_i\beta_j + \alpha_i\delta_k + \beta_j\delta_k + \epsilon_{ijkl}; \quad (3)$$

where:

$\mu = response\ means$

$\alpha_i = effect\ of\ infill\ density, for\ i = 1,2,3$

$\beta_j = effect\ of\ layer\ height, for\ j = 1,2$

$\delta_k = effect\ of\ print\ speed, for\ k = 1,2$

$\alpha_i\beta_j, \alpha_i\delta_k, and\ \beta_j\delta_k\ = interaction\ terms$

$\epsilon_{ijkl} = error\ term,\ l = 1,2,\ldots,48$

Then the analysis refers to the Wilks' Lambda [31] F-values and P-values shown in Table 3 to determine the significance of the input variable to all response variables. We can also refer to the corresponding MANOVA tables that take the correlation effects into account for input variables and their interactions. Similar to the correlation coefficients, significance will also be selected based off a P-value less than 0.05, as is common. The MANOVA calculations show that each input variable is significant to the response variables overall. A higher F-value signifies a greater significance than a lower F-value, as a higher F-value correspondingly creates a lower P-value. As shown by the computed F-values, the order of most influencing input variable is layer height, followed by print speed, followed by infill density.

Table 3: MANOVA Wilks' Lambda Overall Effect Analysis, note that the P-value is the value in the Pr > F column

MANOVA Wilks' Lambda Statistics for Hypothesis of No Overall Effect					
Source	**Value**	**F-Value**	**Num DF**	**Den DF**	**Pr > F**
Infill Density Wilks' Lambda	0.02114802	22.97	22	86	<.0001
Layer Height Wilks' Lambda	0.01327122	290.64	11	43	<.0001
Print Speed Wilks' Lambda	0.06191245	59.23	11	43	<.0001
Infill Density * Layer Height Wilks' Lambda	0.01506289	24.99	22	76	<.0001
Infill Density * Print Speed Wilks' Lambda	0.09027408	8.04	22	76	<.0001
Layer Height * Print Speed Wilks' Lambda	0.25241838	10.23	11	38	<.0001

In order to find the percent influence of an input variable from MANOVA, the following equation is used.

$$R^2 = \left(\frac{n(\Sigma xy) - (\Sigma x)(\Sigma y)}{\sqrt{[n(\Sigma x^2) - (\Sigma x)^2][n(\Sigma y^2) - (\Sigma y)^2]}} \right)^2 \quad (4)$$

As shown in Table 4, all input variables are significant effectors of print time. The most significant variable is the layer height. Based upon the gathered data, print time increases as infill density increases, and 28.16% of the variability within print time data is explained by the infill density. Conversely, print time decreases as layer height increases, and 40.01% of the print time

is explained by layer height. Print time also decreases as the input variable print speed is increased; 21.57% of the variation in the data is determined by print speed. Print time can be minimized by reducing infill density, increasing layer height, and increasing print speed. Approximately 89.75% of the changes in print time within the gathered data are explained by the chosen input variables of infill density, layer height, and print speed. Layer height appears to be the most significant effector based off the data results.

Table 4: Print Time MANOVA Table

Print Time MANOVA					
Source	**DF**	**Type III SS**	**Mean Square**	**F-Value**	**Pr > F**
Model	9	0.74914008	0.08323779	2149.95	<0.001
Error	48	0.00185837	0.00003872		
Corrected Total	57	0.75099846			
Infill Density	2	0.21147094	0.10573547	2731.05	<.0001
Layer Height	1	0.30051101	0.30051101	7761.92	<.0001
Print Speed	1	0.16201685	0.16201685	4184.74	<.0001
Infill Density * Layer Height	2	0.04942905	0.02471453	638.35	<.0001
Infill Density * Print Speed	2	0.00737813	0.00368907	95.29	<.0001
Layer Height * Print Speed	1	0.00192094	0.00192094	49.62	<.0001

As shown in Table 5, all input variables are significant effectors of energy consumption. Infill density accounts for 26.83% of the variation within energy consumption. As infill density increases, energy consumption increases. The data determined that 36.07% of the variation in energy consumption is determined by layer height, making it the most significant input variable affecting energy consumption. When layer height increases, energy consumption decreases. The energy consumption decrease is likely due to the corresponding decrease in print time that reduces the time the machine is running. Print speed accounts for 23.58% of the variability in energy consumption. As print speed increases the trend is that energy consumption decreases. Approximately 86.47% of the changes in energy consumption within the gathered data are explained by the chosen input variables of layer height, infill density, and print speed. Interaction exists between each combination of the input variables. Based upon the gathered data, energy consumption can be minimized by reducing infill density, increasing layer height, and increasing print speed.

Table 5: Energy Consumption MANOVA Table

Energy Consumption MANOVA					
Source	**DF**	**Type III SS**	**Mean Square**	**F-Value**	**Pr > F**
Model	9	0.00581095	0.00064566	222.08	<.0001
Error	48	0.00013955	0.00000291		
Corrected Total	57	0.00595050			
Infill Density	2	0.00159622	0.00079811	274.52	<.0001
Layer Height	1	0.00214642	0.00214642	738.27	<.0001
Print Speed	1	0.00140304	0.00140304	482.58	<.0001
Infill Density * Layer Height	2	0.00042432	0.00021216	72.97	<.0001
Infill Density * Print Speed	2	0.00011381	0.00005690	19.57	<.0001
Layer Height * Print Speed	1	0.00000985	0.00000985	3.39	<.0001

As shown in Table 6, infill density and layer height are significant effectors of mass. Print speed is not a significant effector for mass of the parts. Mass increases as infill density increases, which is the most significant input variable from the data. Infill density accounts for 79.76% of the variability within the response variable of mass. Additionally, mass increases as layer height increases, and 12.38% of the mass variability is explained by layer height. Notably, as layer height increases, the mass appears to vary by a smaller margin. This narrowing may be due to accidental over-extrusion of material that can occur with higher layer heights. It could also be due to the extrusion of more material at once reducing the voids that occur between the layers. Print speed is relatively inconsequential to mass based on the data. Approximately 92.14% of the changes in energy consumption within the gathered data are explained by the chosen input variables of layer height and infill density. Mass can be minimized most effectively by reducing infill density and reducing layer height based on the data. As shown in Table 7, all input variables are significant effectors of magnetic flux density. The most significant variable is the infill density accounting for 81.11% of variation, and it is notably more significant than the other two input variables. This result makes logical sense, as an increase in mass correspondingly increases the total amount of iron within the print, though the percentage remains mostly unchanged. With more iron material within the print, magnetic flux density increases. This observation also supports the high correlation value within the correlation table. Layer height and print speed account for less than 5% of the overall data variation. Magnetic flux density can be increased by increasing infill density and layer height, though infill density is the more relevant of the two. The highest magnetic permeability of any sample was found to be 2.5 Gauss with a sample of 100% infill density, and the lowest magnetic permeability was found to be 0.5 Gauss with samples of 20% infill density.

The samples display a relatively weak magnetic permeability compared to pure iron, though the samples still display enough magnetic properties to attach to magnetized objects.

Table 6: Mass MANOVA Table

Mass MANOVA					
Source	**DF**	**Type III SS**	**Mean Square**	**F-Value**	**Pr > F**
Model	9	25.09033769	2.78781530	1759.44	<.0001
Error	48	0.07605541	0.00158449		
Corrected Total	57	25.16639310			
Infill Density	2	20.07373266	10.03686633	6334.45	<.0001
Layer Height	1	3.11624755	3.11624755	1966.72	<.0001
Print Speed	1	0.01836135	0.01836135	11.59	0.0013
Infill Density * Layer Height	2	1.68689112	0.84344556	532.31	<.0001
Infill Density * Print Speed	2	0.00386459	0.00193229	1.22	0.3044
Layer Height * Print Speed	1	0.00558959	0.00558959	3.53	0.0664

Table 7: Magnetic Flux Density MANOVA Table

Magnetic Flux Density MANOVA					
Source	**DF**	**Type III SS**	**Mean Square**	**F-Value**	**Pr > F**
Model	9	20.4811079	2.27567866	51.36	<.0001
Error	48	2.12665066	0.04430522		
Corrected Total	57	22.6077586			
Infill Density	2	18.3368108	9.16840544	206.94	<.0001
Layer Height	1	0.60600721	0.60600721	13.68	0.0006
Print Speed	1	0.43879052	0.43879052	9.90	0.0028
Infill Density * Layer Height	2	0.34354165	0.17177082	3.88	0.0275
Infill Density * Print Speed	2	0.62379378	0.31189689	7.04	0.0021
Layer Height * Print Speed	1	0.07996699	0.07996699	1.80	0.0664

Dimensional variation did not show correlation with other output variables. Input variables were not significant effectors on width or length, but input variables were found to be significant upon the height of the samples.

Table 8 shows that none of the P-values of any input variables fall below the 0.05 threshold, signifying that no input variable is significant to the dimensional variation of length. This is supported by the regression analysis within, which also shows the same trend. Variables other than the chosen input variables are much more significant in determining the dimensional variation along the length or y-axis. On average, the data showed that length appears to be around 0.6% under the original designed length.

Table 8: Length MANOVA Table

Length Variation MANOVA					
Source	**DF**	**Type III SS**	**Mean Square**	**F-Value**	**Pr > F**
Model	9	0.52636765	0.05848529	1.30	0.2604
Error	48	2.15488235	0.04489338		
Corrected Total	57	2.68125000			
Infill Density	2	0.08905995	0.04452998	0.99	0.3783
Layer Height	1	0.08268368	0.08268368	1.84	0.1811
Print Speed	1	0.04397386	0.04397386	0.98	0.3273
Infill Density * Layer Height	2	0.05735803	0.02867902	0.64	0.5323
Infill Density * Print Speed	2	0.23263542	0.11631771	2.59	0.0854
Layer Height * Print Speed	1	0.00188235	0.00188235	0.04	0.8386

Table 9 shows that none of the P-values of any input variables fall below the 0.05 threshold, signifying that no input variable is significant to the dimensional variation of width. This lack of significance is supported by the regression analysis, which also shows the same trend. Variables other than the chosen input variables are more significant in determining the dimensional variation along the x-axis. On average, the data showed that length appears to be around 0.223% under the original designed width. As shown in Table 10, all of the input variables are significant effectors to the material height dimensional variation. However, though they are significant effectors, the regression analyses show that the effect is roughly only 5% of the variation within the data. While the input variables are significant, it seems likely that variables other than the chosen input variables are much more significant in determining the dimensional variation in the height. Notably, the height appears to be about 7.7% over the designed height on average, which is less accurate than either of the width or length dimensions. The inaccuracy in height is also notable for height being the only dimension that is over the designed parameters on average, where width and length variations were slightly under.

Table 9: Width MANOVA Table

Width Variation MANOVA					
Source	**DF**	**Type III SS**	**Mean Square**	**F-Value**	**Pr > F**
Model	9	0.17644234	0.019860470	1.32	0.2539
Error	48	0.71516327	0.01489923		
Corrected Total	57	0.89160560			
Infill Density	2	0.04182952	0.02091476	1.40	0.2556
Layer Height	1	0.02815625	0.02815625	1.89	0.1756
Print Speed	1	0.00317681	0.00317681	0.21	0.6463
Infill Density * Layer Height	2	0.03641847	0.01820923	1.22	0.3036
Infill Density * Print Speed	2	0.05676618	0.02838309	1.91	0.1599
Layer Height * Print Speed	1	0.00567681	0.00567681	0.38	0.5400

Table 10: Height MANOVA Table

Height Variation MANOVA Table					
Source	**DF**	**Type III SS**	**Mean Square**	**F-Value**	**Pr > F**
Model	9	43.9373732	4.8819304	0.59	0.7960
Error	48	394.9117647	8.2273284		
Corrected Total	57	438.8491379			
Infill Density	2	19.45842760	9.72921380	1.18	<.0001
Layer Height	1	0.07597114	0.07597114	0.01	0.0006
Print Speed	1	3.46699346	3.46699346	0.42	0.0028
Infill Density * Layer Height	2	11.46227376	5.73113688	0.70	0.0275
Infill Density * Print Speed	2	5.11534641	2.55767320	0.31	0.0021
Layer Height * Print Speed	1	4.24705882	4.24705882	0.52	0.0664

Surface Roughness shows significant correlation with different input variables depending on the surface. For simplicity of documentation, a surface may also be referred to as a face for this document. As shown in Table 11, layer height, print speed, and infill density are significant effectors to the Surface Roughness on the top of the print. Though the infill density is shown to be

significant from the MANOVA, the analysis that infill density appears to have less than a 1% influence on the variation of the data. Around 62.61% of the variation in Surface Roughness of the top face is accounted for by layer height. The data also shows that a lower layer height corresponds to a less rough surface for the top of a print. Another 6.67% of the variation appears to come from the input variable of print speed according to the regression. Most of the remaining variation comes from other effectors. Based on the data, for Surface Roughness of the top surface of a print, layer height should be kept low along with print speed.

Table 11: Surface Roughness of Top Face MANOVA Table

Surface Roughness of Top Face MANOVA Table					
Source	**DF**	**Type III SS**	**Mean Square**	**F-Value**	**Pr > F**
Model	9	15.53125608	1.72569512	21.41	<.0001
Error	48	3.86893242	0.08060276		
Corrected Total	57	19.40018850			
Infill Density	2	0.55290433	0.27645216	3.43	0.0405
Layer Height	1	12.14810694	12.14810694	150.72	<.0001
Print Speed	1	1.29530060	1.29530060	16.07	0.0002
Infill Density * Layer Height	2	0.65251634	0.32625817	4.05	0.0237
Infill Density * Print Speed	2	0.20721636	0.10360818	1.29	0.2859
Layer Height * Print Speed	1	0.72142594	0.72142594	8.95	0.0044

As shown Table 12, the only input variable that is a significant effector to the Surface Roughness on the length face or y-axis of the print is layer height. Infill density does not display much of an affect upon Surface Roughness along the length face. The data appears to show that increasing layer height can help reduce Surface Roughness on the length face, though only 10.34% of the variation within that data appears to be from the layer height. The data shows a nearly negligible impact from print speed. Based on the table, layer height has a slight impact on the Surface Roughness along the length face, but some other variables other than the chosen input variables are much more significant in determining the Surface Roughness.

Table 12: Surface Roughness of Length Face MANOVA

Surface Roughness of Length Face MANOVA Table					
Source	**DF**	**Type III SS**	**Mean Square**	**F-Value**	**Pr > F**
Model	9	9.39375195	1.04375022	1.65	0.1270
Error	48	30.29465861	0.63113872		
Corrected Total	57	39.68841057			
Infill Density	2	1.97908916	0.98954458	1.57	0.2190
Layer Height	1	4.10544906	4.10544906	6.50	0.0140
Print Speed	1	0.00033120	0.00033120	0.00	0.9818
Infill Density * Layer Height	2	1.78263517	0.89131759	1.41	0.2535
Infill Density * Print Speed	2	0.30894059	0.15447029	0.24	0.7839
Layer Height * Print Speed	1	0.93708000	0.93708000	1.48	0.2290

As shown Table 13, the only input variable that is a significant effector to the Surface Roughness on the width or x-axis of the print is infill density. Even then, a majority of the variation appears to be uncontrolled. Most likely, other factors other than the chosen input variables that are much more significant in determining the Surface Roughness.

Table 13: Surface Roughness of Width Face MANOVA

Surface Roughness of Width Face MANOVA Table					
Source	**DF**	**Type III SS**	**Mean Square**	**F-Value**	**Pr > F**
Model	9	19.64352603	2.18261400	2.26	0.0335
Error	48	46.32671838	0.96513997		
Corrected Total	57	65.97024441			
Infill Density	2	14.01314077	7.00657038	7.26	0.0018
Layer Height	1	0.00527431	0.00527431	0.01	0.9414
Print Speed	1	3.11169044	3.11169044	3.22	0.0789
Infill Density * Layer Height	2	0.79215124	0.39607562	0.41	0.6657
Infill Density * Print Speed	2	0.62537204	0.31268602	0.32	0.7248
Layer Height * Print Speed	1	0.31910598	0.31910598	0.33	0.5680

Discussion

This study reveals a number of findings. Overall, all input variables are significant to the output responses as a whole. Layer height is the most influencing input variable. Print speed is the second most influencing. And, infill density is the third most influencing overall. The other key findings could be listed as follows:

- There is significant correlation among print time, print cost, magnetic flux density, and mass.
- Print time and print cost are very highly correlated to one another.
- Mass and magnetic flux density are highly correlated with one another.
- Energy consumption, cost, and print time all increase as the input variables of infill density increases, layer height decreases, and print speed decreases.
- While all input variables are significant to them, mass and magnetic flux density are most significantly affected by infill density and increase as infill density increases.
- With this material, light weighting is not feasible if the main goal is to have a part with decent magnetic flux density.
- Dimensional accuracy of the prints is poorest in the z-direction when compared to the x or y direction.
- Only dimensional accuracy in the z-direction appears to be significantly affected by the input variables.
- Surface Roughness of the width and length faces appear to be influenced less than 15% by the input variables based off the data.
- Surface Roughness of the top face is most significantly affected by layer height.
- All input variables were significant for the data as a whole according to MANOVA.

It is proven that the parts produced with Iron-PLA composite filament presents enough level of magnetability to hold metallic work pieces. While the strength is relatively low, the part is capable of connecting to a magnet. This allows for a reduction in post processing, as fewer magnets are necessary to be injected within an object. With the analysis of the printed specimens, data has been generated on changes that can improve response parameters. In regards to magnetic flux density, testing has shown that having a 100% infill density is the most significant factor. Through printing a spare parts holder design, the holder can be tested if the 20% Iron-PLA composite filament displays ferromagnetic properties. The print shows that the design is satisfactory for holding a magnetic connection to a magnetized object. The sample is capable of holding against its own weight, and can additionally hold some small additional weight on the other end of the magnet as well. While the magnetic flux density would be improved with a higher percentage of iron within the PLA, the material, and any parts manufactured with the material, are still responsive within a magnetic field. Though care should be taken, as while the material will respond to a magnetic field, the response is weak when compared to pure iron. The current investigation shows that the parameters producing quality Iron-PLA parts are

- 100% infill density
- 0.1 mm layer height
- 45 mm/s print speed

These parameters are used to produce a real-life scenario for a spare parts holder. Figure 4 shows a side view of the spare parts holder. Figure 5 shows the spare parts holder successfully resisting the force of gravity acting upon the spare parts holder and the additional weight.

Figure 4: Additively Manufactured Iron-PLA Spare Parts Holder – Side View

Figure 5: Additively Manufactured Iron-PLA Spare Parts Holder – In Action

Conclusion and Future Work

This research study is focused to collect a number of knowledge elements related to the Iron-PLA filaments which could be used for fabricating magnetic workpieces for real life applications. The collected data shows that the input variables of infill density, layer height, and print speed are significant for the response variables of energy consumption, mass, magnetic flux density, and print time, but are not as significant for dimensional variation and Surface Roughness. According to MANOVA, the most substantial effector of the response variables is the input variable of layer height. The second most substantial effector of the data is the input variable of print speed. The least substantial input variable from this data in terms of effect on response variables is infill density, though the effect is still significant.

The data analysis shows that print time can be reduced through reducing infill density, increasing layer height, and increasing print speed. Energy consumption and cost can be reduced through reducing infill density, increasing layer height, and increasing print speed. Mass can be reduced through decreasing infill density and layer height. Dimensional accuracy is significantly affected only by the chosen input variables in the z-direction of the printed samples. The x and y directions of the print are largely unaffected by the input variables. Surface Roughness along the top surface of an object appears to be significantly affected by layer height. While the data shows the impact of input variables on the Surface Roughness along the length and width faces of the print, other unaccounted factors impact them more effectively. The Iron-PLA spare parts holder fabricated with parameters of 100% infill density, 0.1 mm layer height, and 45 mm/s print speed shows that an additively manufactured magnetable part could be made. The functional testing of the spare parts holder proves that the holder could be used for storing nails, washers, bolts, and nuts in a machine shop environment.

In future works, response surface methodology could be utilized in addition to this data to further improve a desired response variable. The current study could also be expanded with the addition of extra knowledge blocks generated from different Iron-PLA composite filaments and process parameters.

Acknowledgements

This work has been made possible by the research assistantship provided by the National Science Foundation Award Number 1801120, “Smart Manufacturing for America's Revolutionizing Technological Transformation.”

References

[1] Hasanov, S., et al. "Review on Additive Manufacturing of Multi-Material Parts: Progress and Challenges." *J. Manuf. Mater. Process* 6.4 (2022).

[2] T. Wohlers, N. Mostow, I. Campbell, O. Diegel, J. Kowen, I. Fidan, “Wohlers Report 2022,” pp. 128, ISBN: 978-0-9913332-9-5, ASTM International, 2022.

[3] Tümer, H. Eda, and Husnu Y. Erbil. (2021). "Extrusion-Based 3D Printing Applications of PLA Composites: A Review." *Coatings* 11, no. 4: 390. https://doi.org/10.3390/coatings11040390.

[4] B. Blakey-Milner, P. Gradl, Snedden G., Brooks M., Pitot J., Lopez E., ... & du Plessis, A. (2021). Metal additive manufacturing in aerospace: A review. *Materials & Design*, *209*, 110008.

[5] Ulu E., Huang R., Kara L. B., & Whitefoot K. S. (2019). Concurrent structure and process optimization for minimum cost metal additive manufacturing. *Journal of Mechanical Design*, 141(6).

[6] Terry, Shane, et al. "The influence of smart manufacturing towards energy conservation: a review." *Technologies* 8.2 (2020): 31.

[7] Chaudhary V., Mantri S. A., Ramanujan R. V., & Banerjee R. (2020). Additive manufacturing of magnetic materials. *Progress in Materials Science*, *114*, 100688.

[8] Najgebauer, Mariusz & Szczyglowski, Jan & Ślusarek, Barbara & Przybylski, Marek & Kaplon, Andrzej & Rolek, Jaroslaw. (2018). Magnetic Composites in Electric Motors. 10.1007/978-3-319-63949-9_2.

[9] Lauren Henderson, Sam Zamora, Tanjina N. Ahmed, Camila Belduque, Jitendra Tate, Maggie Yihong Chen, Wilhelmus J. Geerts. “Altering magnetic properties of iron filament PLA using magnetic field assisted additive manufacturing (MFAAM).” *Journal of Magnetism and Magnetic Materials*, Volume 538, 2021, 168320, ISSN 0304-8853, https://doi.org/10.1016/j.jmmm.2021.168320.

[10] Watson N. D., & Von Lockette P. (2018). Deposition Controlled Magnetic Alignment in Iron-PLA Composites. (2018) *International Solid Freeform Fabrication Symposium*. University of Texas at Austin.

[11] Guan, Xiao-Na, et al. "Electromagnetic and mechanical properties of carbonyl iron powders-PLA composites fabricated by fused deposition modeling." *Materials Research Express* 5.11 (2018): 115303.

[12] Angelopoulos P. M., Samouhos M., & Taxiarchou M. (2021). Functional fillers in composite filaments for fused filament fabrication; a review. *Materials Today: Proceedings*, *37*, 4031-4043.

[13] Lu H. (2020). *Preliminary Mechanical Characterization of the Low-Cost Metal 3D Printing* (Master Thesis, Tennessee Technological University).

[14] Bade, Lokesh, et al. "Investigation into the development of an additive manufacturing technique for the production of fibre composite products." *Procedia engineering* 132 (2015): 86-93.

[15] Maurel A., Haukka M., MacDonald E., Kivijärvi L., Lahtinen E., Kim H., ... & Panier, S. (2021). Considering lithium-ion battery 3D-printing via thermoplastic material extrusion and polymer powder bed fusion. *Additive Manufacturing*, *37*, 101651.

[16] Murr L. E., Martinez E., Amato K. N., Gaytan S. M., Hernandez J., Ramirez D. A., & Wicker R. B. (2012). Fabrication of metal and alloy components by additive manufacturing: examples of 3D materials science. Journal of Materials Research and technology 1.1: 42-54.

[17] Femi-Oyetoro J. D. (2021). *Prediction of Flexural Properties for Additively Manufactured Short Carbon Fiber Reinforced Composites Using Machine Learning Techniques* (Master Thesis, Tennessee Technological University).

[18] Hasanov, Seymur, and Ismail Fidan. "Manufacturing of Soft Magnets using the Fused Filament Fabrication Process." *MatEDU Resource Center* (2020).

[19] SolidWorks 2021. (2021) https://www.solidworks.com/ Retrieved June 13, 2022

[20] Wong, Kaufui V., and Aldo Hernandez. "A review of additive manufacturing." ISRN Mechanical Engineering. v. 2012. Article ID 208760. (2012).

[21] Dremel DigiLab 3D Slicer. https://www.dremel.com/gn/en/digilab/software Retrieved June 13, 2022.

[22] Dremel Digilab 3D Printer 3D45. https://www.dremel.com/gn/en/p/dremel-digilab-3d-printer-3d45-3d45-01-v724 Retrieved June 13, 2022.

[23] AMOLEN 3D Printer Filament (20% Magnetic Iron Powder - PLA Filament 1.75mm). https://amolen.com/ purchased through Amazon https://www.amazon.com/AMOLEN-Filament-Magnetic-Contains-Polishing/dp/B09CPHBZGV/ref=sr_1_3?crid=1QF7O4EEDHTUN&keywords=magnetic+iron+pla&qid=1655132886&sprefix=magnetic+iron+pla%2Caps%2C70&sr=8-3. February, 2022.

[24] Clock Application, https://www.samsung.com/us/. Retrieved June 13, 2022.

[25] *Reed R5090 power meter*. GlobalTsetSupply.com. (n.d.). https://www.globaltestsupply.com/product/reed-r5090-power-meter?gclid=CjwKCAjw6dmSBhBkEiwA_W-EoMjx04Vxuex5f9J2UpF0o4O438zaTQuGmf-UHrTr95u7veIaEe2wORoCnywQAvD_BwE. Retrieved April 19, 2022.

[26] Local Energy Price, https://www.cookeville-tn.gov/220/Retail-Electric-Rates. Retrieved January 2022.

[27] Mettler Toledo. PL602-s. https://www.mt.com/my/en/home/products/Laboratory_Weighing_Solutions/Precision_Balances/Standard/PL-E_Precision/PL602E.html, Retrieved June 12, 2022.

[28] IP54 Digital Calipers. https://eagems-llc.com/pages/eagems-digital-caliper-ip54. Retrieved June 13, 2022.

[29] Mitutoyo (2016). SJ-210. https://www.mitutoyo.com/products/form-measurement-machine/surface-roughness/sj-210-portable-surface-roughness-tester-2/. Retrieved June 12, 2022.

[30] FW Bell Model 640 Gaussmeter. (2017) https://fwbell.com/wp-content/uploads/2017/11/UN1006.pdf. Retrieved June 13, 2022.

[31] French, Aaron, et al. "Multivariate analysis of variance (MANOVA)." (2008).

[32] Stephanie Glen. "Wilks' Lambda: Simple Definition." From StatisticsHowTo.com: Elementary Statistics for the rest of us! https://www.statisticshowto.com/wilks-lambda/.